Weather Radar Receiver Identification for Improving Wi-Fi Interference Detection

Jorge Cogo*†, Arturo Collado Rosell‡†, Javier A. Areta*†§, and Juan P. Pascual†§
* Universidad Nacional de Río Negro. CITECCA. Anasagasti 1463, Bariloche, Argentina.
† Instutito Balseiro. Universidad Nacional de Cuyo, Av. Bustillo 9500, Bariloche, Argentina.
‡ Comisión Nacional de Energía Atómica (CNEA), CAB, Av. Bustillo 9500, Bariloche, Argentina.
§ Consejo Nacional de Investigaciones Científicas y Técnicas (CONICET).
emails: {jcogo, jareta}@unrn.edu.ar, {arturo.collado, juanpablo.pascual}@ib.edu.ar

***Abstract*—One of the main sources of electromagnetic interference that affects the operation of weather radars is due to Wi-Fi networks that operate in the same frequency band.**

There are various signal processing strategies to mitigate the interference effect. One of these strategies is to detect the signal using the deterministic preamble of the Wi-Fi packets.

This work presents a radar receiver identification technique that allows generating a reference signal that better assimilates the preamble received in the processing stage and therefore helps to improve the method for detecting these interfering signals.

***Index Terms*—Weather Radar, System Identification, Wi-Fi**

I. Introduction

The weather radar is currently a fundamental tool for observing the atmosphere and making short- and medium-term forecasts [1], [2]. Its potentiality for observing large regions of space in a short time (and the neccesary sensitivity of the receiver), however, makes it susceptible to being interfered by the electromagnetic signals present in these regions. For radars operating in C-band, such as the Argentine Meteorological Radar (RMA) [3], the greatest source of interference is due to RLAN/WLAN transceivers [4]. Almost all of the installed WLAN devices are based on the IEEE 802.11 standard, and are commonly called Wi-Fi [5].

This interference problem is global in scope. In [4] the authors give examples of radars from the USA, Argentina and South Africa, while in [6] the authors present a survey on RLAN interferences captured by Canadian weather radars. In [7] the authors report the results of interference studies in a radar of the TDWR network (Terminal Doppler Weather Radar) of Puerto Rico, thoroughly analyzing the interfering signals present at different stages of the radar reception chain. In [8] the authors expose the growth in interference recorded by radars in northwestern Italy between 2010 and 2014.

Broadly speaking, the weather radar operates by transmitting electromagnetic energy in the form of pulses, and receiving the signal reflected from the objects of interest. In the time interval between two pulses, called the observation window, N *samples* are taken. Each sample corresponds to a distance or range relative to the radar. These samples are the input for signal processing stages, and in order to optimize the Signal to Noise Ratio (SNR), they are obtained at the output of a matched filter or a correlator. For practical considerations, a quadrature receiver is used, and each IQ sample is generally represented by a complex number [2].

In the most common operating mode, the radar performs this procedure while rotating on its vertical axis, keeping the elevation fixed for at least one complete turn. Thus, the antenna points to a different azimuth (and the same elevation) for each transmitted pulse. When the radar completes 360 degrees of rotation, which is called a complete scan, M transmitted pulses elapsed, with N taken samples each, which can be ordered as an $M \times N$ matrix of complex numbers. The dimension in which the M pulses are transmitted is called azimuth dimension, while the dimension where the N samples are taken is called the range dimension. In dual polarization radars, this operation is simply doubled for horizontally polarized and vertically polarized transmitted pulses, obtaining two matrices of $M \times N$ samples [1], [9]. We refer to these two polarizations as HH and VV, respectively.

Ideally, each IQ sample contains information on the backscatter of the transmitted pulse in hydrometeors, if any (signal of interest), and on the backscatter of the transmitted pulse on surrounding objects such as insects and birds, buildings, trees, mountains, etc., if any (unwanted signal, called *clutter*), and noise. When in the scanning process, the radar points in the direction where there is a Wi-Fi transceiver operating in the same band, it is very likely that this signal will be received by the radar. This signal will appear as additive interference, affecting the samples in the observation window that coincide in time with part or all of each Wi-Fi packet. That is, for each Wi-Fi packet (or a fraction of it) that is captured, n_i samples will be interfered in the range dimension (n_i consecutive elements of the corresponding data matrix row).

At the processing stage, observations from several consecutive pulses (called the Coherent Processing Interval, CPI) are combined to reduce the dispersion of the estimates. Even if only a few samples are affected by interference, this interference will affect the estimator. For example, the effect of interference appears as high-amplitude radial lines on the Plan Position Indicator (PPI) for reflectivity [4]. To a different extent, the interference affects all the Doppler and polarimetric products generated by the radar, resulting in biases in, for example, the hydrometeor classification and

quantitative precipitation estimation [8].

There are different solution proposals from the point of view of signal processing. In [10] the authors present a mitigation method based on spectral decomposition that incorporates polarimetric information and uses image processing techniques and a fuzzy logic classification algorithm. In [11] the authors carry out a study of WLAN/RLAN and measure 802.11a, g and n OFDM signals, with the aim of improving existing techniques or developing new ones that allow their recognition in the context of weather radar.

In [12] the author proposes a 2D interference filtering algorithm, using the range/pulse domains; allowing detections in lower interference-to-noise or interference-to-signal ratios compared to filters that operate in only one dimension. In [13] the authors present an interference identification method based on fuzzy logic, which uses polarimetric observables, and a spatial filter to replace the contaminated pulses.

In the works of [14] and [15] they propose filtering techniques based on the wavelet transform and other discrete filter variants. In [16] and [17] a Neyman-Pearson detection scheme for the preamble of the Wi-Fi signal at the output of the matched filter, exploiting the deterministic structure of the preamble, is proposed.

One of the disadvantages of the preamble detection method proposed in [16] and [17] is that it assumes an overly simplified model of the processing that the radar performs on the received interfering signal. In this work, we present an improvement in the detection of Wi-Fi signals on weather radar data, based on obtaining a reference signal that better approximates the observed preamble by identifying the processing that the radar performs on the signal.

In section II we describe in more detail the structure of radar reception stages, and present the identification method and the results on real data. In section III we present an alternative detection technique based on power levels that allows us to obtain test signals from real data, and briefly describe how we obtain the reference signals for detection. In Section IV we present the detection results on these test signals using the correlation coefficient as a performance metric. Finally, in section V we drawn the conclusions.

The analysis of the results is carried out exclusively with real data, obtained from the RMA1 located in the city of Córdoba, Argentina, a dual-polarization Doppler weather radar that operates in C-band [3].

II. System Identification

A. Receiver Structure

The pulses transmitted by the radar are modulated by a high frequency carrier, and therefore the signal observed at the antenna terminals in reception mode is also at high frequency. For practical reasons, the matched filter is not implemented directly at this high frequency. In general, the radar receiver has the following stages: first an RF filter and low noise amplifier (LNA), then a mixer to shift the signal to a lower intermediate frequency (IF) followed by an IF filter, and finally a matched filter. In general, after the IF filter, the signals are digitized, and the matched filter is digitally implemented. Furthermore, to preserve phase information after conversion to IF, two branches in-phase (I) and in-quadrature (Q) are used. The matched filter output, sampled at a given rate T_s, is the input for signal processing stages, as was succinctly described in section I.

All this processing (partly analog, partly digital) that is performed on the received signal will also modify the interfering Wi-Fi signal. That is why we are interested in identifying the behavior of these stages.

To simplify this identification, we assume (first hypothesis) that the behavior of these stages can be modeled by a Linear Time-Invariant (LTI) system. Although, there are two important reasons to question the validity of this assumption. First, the mixing stage is a time-varying system. However, by interpreting the entire system in terms of equivalent low-pass signals, this mixing process can be factored out. It should be remembered that the mixing stage is placed between two filter stages (RF and IF) for practical considerations. Mathematically, it can be replaced by a single equivalent filtering stage and a pre or post shift in frequency.

Second, the output of the matched filter is sampled at a lower frequency than the input. There is therefore an implicit decimation stage in the signal. This decimation will have to be contemplated at some point, as we will see.

Furthermore, we assume (second hypothesis) that the noise component that affects the radar input signal can be modeled as Additive White Gaussian Noise (AWGN). This is a widely used and accepted model [2].

B. Method

Assuming an LTI system with frequency response $H(f)$ and AWGN with Power Spectral Density (PSD) $S_{XX}(f) = {}^{N_0}/_2$ as input signal, the PSD of the output, $S_{YY}(f)$, is [18]

$$S_{YY}(f) = \frac{N_0}{2}|H(f)|^2. \tag{1}$$

The procedure consists in identifying consecutive sample sets corresponding to AWGN-only input, and then obtaining an estimate of the output PSD, $\hat{S}_{YY}(f_i)$ at discrete frequencies f_i. Starting from a complete scan data record taken in a condition of no meteorological phenomenon present (a clear sky day), we have the aforementioned $M \times N$ complex data matrix. In this condition, each sample can contain a combination of clutter, noise, and Wi-Fi interference. Then:

1) We take groups of K consecutive rows (azimuth dimension), so partitioning the $M \times N$ matrix into M/K smaller matrices of dimension $K \times N$. K is selected such as the number of rows in these new matrices coincide with the number of samples in a CPI.
2) We obtain an $\hat{S}^{(k)}_{YY}(f_i)$ estimate for each $K \times N$ data matrix following the next procedure.
   a) We choose an integer L small compared to N, and multiple of R (another integer, defined in *Test A*).
   b) We partition each row into as many as possible non-overlapping sets of L consecutive samples. We obtain $K \cdot \lfloor N/L \rfloor$ sets.

c) We keep only the sets that pass the *Test A* and *Test B* described below.
d) Using periogram [19], we estimate the PSD from each record of L samples, $\hat{S}_{YY}^{(k,\ell)}(f_i)$, $f_i = i/(L \cdot T_s)$, $i \in \mathbb{Z}$, $0 \leq i \leq L-1$.
e) We obtain $\hat{S}_{YY}^{(k)}(f_i)$ by averaging these $\hat{S}_{YY}^{(k,\ell)}(f_i)$ estimates.

3) We keep only the estimates $\hat{S}_{YY}^{(k)}(f_i)$ that were obtained with a significant number of sets.
4) We calculate the median of these estimates $\hat{S}_{YY}^{(k)}(f_i)$ for each frequency f_i, and we keep only those estimates that on average (over all f_i) deviate less than a given threshold U_S from that median.
5) We obtain $\hat{S}_{YY}(f_i)$ averaging these $\hat{S}_{YY}^{(k)}(f_i)$ estimates.

The idea of *Test A* is to keep only the sets in which no large power variations are observed. These large power variations are associated, with a high probability, to a part of the samples containing clutter or interference. In *Test A* we do the following:

1) We partition each set of L samples into R non-overlapping subsets of L/R samples, and calculate the average power over each of these R subsets.
2) We take the ratio between the maximum and the minimum of these R power values.
3) We keep only the sets of L samples whose value of this quotient is less than a threshold U_{P_A}.

However, it could be the case of sets whose samples correspond to clutter or interference but do not present these large variations in power. However, these sets will exhibit higher power due to clutter or interference contributions. The idea of *Test B* is to discard those records with higher power. In *Test B* we do the following

1) We estimate the power over each set of L samples that passed *Test A*.
2) We take $\log_{10}$ of these powers and sort these values.
3) We fit a line with the values belonging to deciles 2 to 4.
4) We keep only the samples that do not deviate more than U_{P_B} from this line.

Certainly, in *Test B* a rough approximation is used, and in the future it could be improved by adjusting the theoretical power distribution for the noise-only case and discarding the values that deviate too much from it.

These two tests are inspired by the procedure described in [20], with the difference that here we want to obtain sets of consecutive samples that correspond to input noise, not isolated samples.

C. Results

We take a complete scan dataset with $M = 19440$, $K = 54$, $N = 4800$ observed in a clear sky day. Figure 1 shows the instantaneous power values (in logarithmic scale) of a row of the data matrix, for the HH polarization. This corresponds to the signal observed for a given transmitted pulse. Approximately from $n = 0$ to $n = 1200$ the presence of clutter is observed, while approx. from $n = 2000$ to $n = 2400$ and from $n = 3200$ to $n = 3400$ the presence of two interference packets is observed. The remaining samples correspond to noise-only input. For VV polarization the results are similar.

The figure also shows the sets of L samples that passed the tests and so are used in the system identification, setting $L = 80$, $R = 4$, $U_{P_A} = 3$ dB, $U_{P_B} = 0.25$ dB. It can be seen that these sets fall into the noise-only zone. The fact that they are so few is due to the chosen thresholds. However, on average 850 sets are obtained, and used to estimate each $\hat{S}_{YY}^{(k)}(f_i)$.

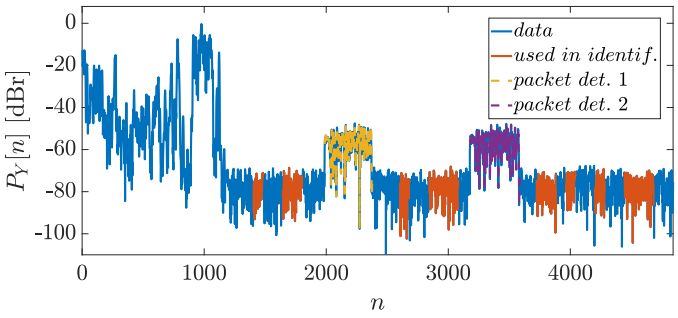

Fig. 1. Instantaneous power in logarithmic scale of the receiver data for a unique transmitted pulse. HH polarization.

Figure 2 shows the resulting estimate of $|H(f_i)|^2$ versus the normalized frequency $f_i \cdot T_s$, for both polarizations HH and VV. This estimate is obtained by solving eq. (1) considering that the maximum value of $|H(f_i)|^2$ is equal to 1.

It can be seen that the estimates in both polarizations are similar, which makes sense since the hardware used in both branches is similar. Although only the case $L = 80$ is shown, for other values of L, the results obtained are similar. This value is a good balance between resolution of the frequency response and the number of sets included in each estimate.

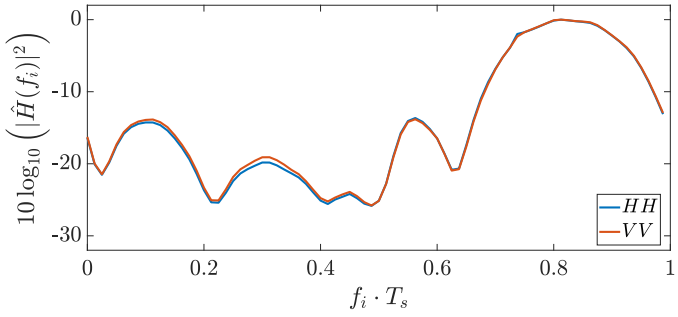

Fig. 2. Estimation of the square of the modulus of the filter in each of the two polarizations, HH and VV. Logarithmic scale.

The resulting system filter is complex in that it processes complex samples (IQ) and results in complex samples (IQ). The filter is band-pass, reflecting the fact that frequency translation does not necessarily drive the signal to zero frequency. From these estimations, we obtain $|\hat{H}(f_i)|$. Since the method does not allow to obtain the filter phase, we will assume that it is linear in order to obtain $\hat{H}(f_i)$. Certainly, the latter is a strong assumption, considering that part of the processing is

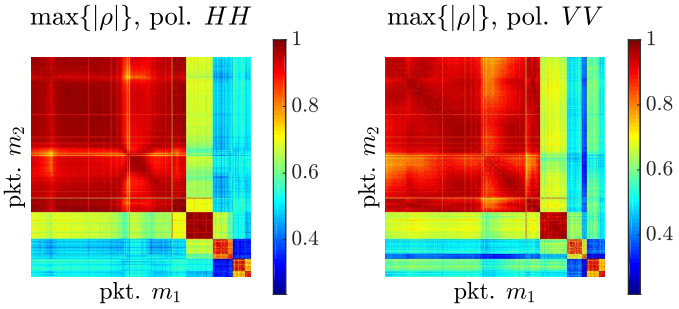

Fig. 3. Maximum modulus of the correlation coefficient between the preambles of each pair of detected packets in each one of the two polarizations. m_1 and m_2 denote two particular packets.

carried out with analog filters. However, we will see that the results obtained seem to indicate that the assumption is valid, at least as a first approximation.

III. Preamble Detection

A. Test packets

In order to obtain test packets, we implemented an alternative ad-hoc detection method based on power levels. This method is based on the following steps.

1) We take moving average of the instantaneous power of each row of the data matrix, with a 10 samples window.
2) For each row, we indicate detection in those indices where this moving average is greater than both adjacent rows moving average corresponding indices by more than 10 dB.
3) For each row, we filter out sparse false detections (due to noise or clutter) of a few consecutive samples.
4) For each row, we fix missdetections of few samples surrounded by many detections.
5) We extend the edge of detection back and forth, looking for big changes in power levels.
6) Since we are particularly interested in the preamble for each packet, packets whose detection begins very close to the clutter zone or very close to the beginning of the row are discarded.
7) We carry out this procedure for the data HH and VV. In order to minimize false detections, we keep only the detections that are observed in both HH and VV in nearby indices.

Figure 1 shows two detected packets with this procedure. With this method we detected a total of 400 packets over a complete scan.

Figure 3 shows the maximum modulus of the correlation coefficient between the preambles of each pair of detected packets. On the one hand, it can be seen that there is consistency in the detected packets, as each preamble exhibits a high degree of correlation to a lot of other preambles. On the other hand, it can be seen that this similarity occurs by groups of detected packets. This is partly due, as we shall see, to the frequency deviation of the respective transmitters.

B. Reference Signal

We will focus on the structure of the Orthogonal Frequency-Division Multiplexing (OFDM) signal that complies with the IEEE802.11a standard, and is transmitted in the 5 GHz band. Although there are other variants of IEEE802.11 that also operate in 5 GHz, due to the number of devices installed, IEEE802.11a is the one that occurs almost exclusively in observed data records. For simplicity we refers to it simply as Wi-Fi.

Being part of a packet switching communication system, in the Wi-Fi transmission scheme, the data are segmented into packets for transmission, and each packet is individually transmitted over the wireless medium [5]. Before transmission, additional symbols are added to each data packet for synchronization, error correction, etc. In particular, a *preamble* is added at the beginning so the receiver can perform the necessary detection and synchronization operation. The preamble is composed of a set of known symbols so that a receiver can detect the start of an incoming packet [21].

To detect the interfering signals we exploit the deterministic structure of the preamble. The details of this structure can be seen in [22]. It is worth clarifying that it is composed of a short symbol training sequence (which we denote STS) followed by a long symbol training sequence (which we denote LTS). We start from this theoretical preamble, with a sampling rate equal to that of the signals entering the matched filter, and we construct three reference signals:

1) We process by an oversimplified matched filter and decimate it, as described in [16] and [17]. In this work we call it the *original reference signal*.
2) We filter this original reference with our estimate of the system filter. We call it the *filtered reference signal version 1 (V1)*.
3) We interpolate the impulse response of our filter estimate so that it has the sample rate of the signals entering the matched filter. With this new filter, we filter the preamble and then decimate the result to the matched filter output rate. We call it the *filtered reference signal version 2 (V2)*.

Note that these three reference signals have the matched filter output sample rate, which is the sample rate of the signals to be processed. The two variants of filtering try to incorporate the effect of the decimation that the signal suffers. Since the filter estimates in HH and VV are very similar, we arbitrarily choose the first of them.

Figure 4 shows the PSD of the original reference signal and of the two filtered reference signals. To simplify the interpretation, we separately plot the PSDs of the STS and the LTS. We also plot the PSD estimated from the samples that would correspond to these preambles in the detected test packets (averaging the PSD estimates from each preamble). To facilitate comparison, each curve is normalized to its maximum value. It can be seen that the frequency content of both filtered reference signals (V1 and V2) resembles much more the frequency content of the test packets than the original

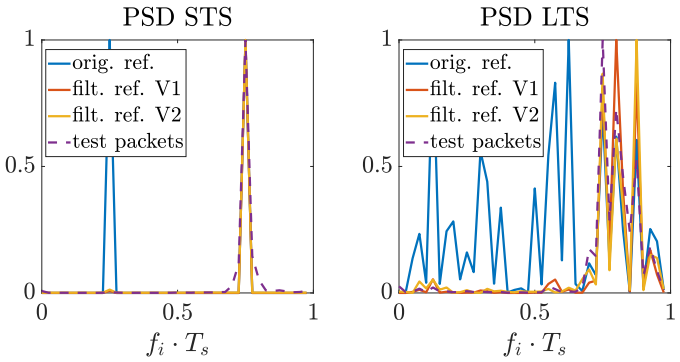

Fig. 4. PSDs of the short and long training sequences of the preamble in the original and filtered references (V1 and V2), and in the test packets (HH).

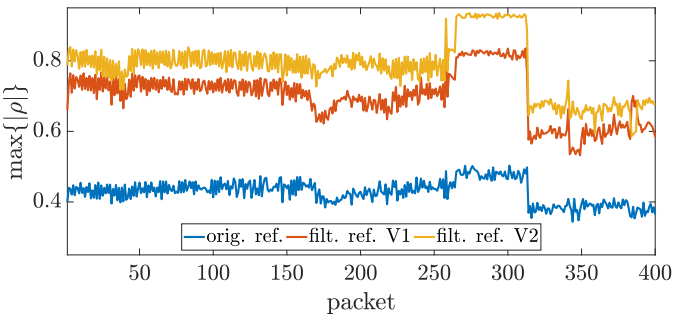

Fig. 5. Maximum modulus of the normalized correlation coefficient between the reference signal and the test Wi-Fi packets, using the original reference and using the filtered references (V1 and V2). HH polarization.

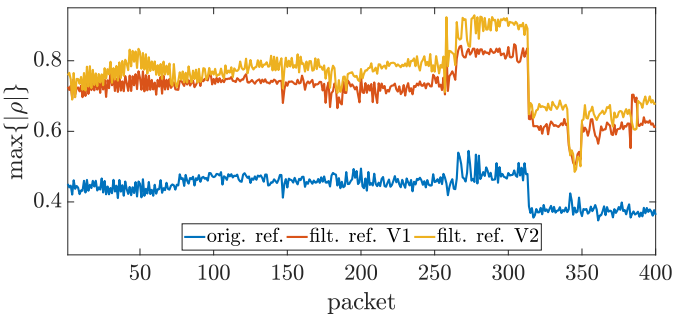

Fig. 6. Maximum modulus of the normalized correlation coefficient between the reference signal and the test Wi-Fi packets, using the original reference and using the filtered references (V1 and V2). VV polarization.

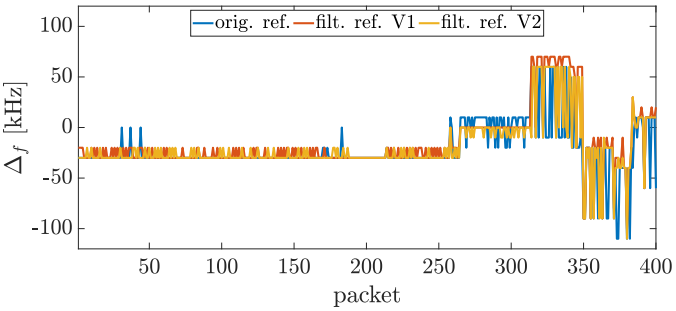

Fig. 7. Frequency error in which the maximum of the correlation coefficient is given for each packet. HH polarization.

reference signal does. It is important to clarify that for the STS PSD the four curves overlap at $f_i \cdot T_s \approx 0.75$.

IV. Results

Figure 5 shows the results of the maximum modulus of correlation coefficient, ρ, between the original reference signal and the previously detected test packets, and between the filtered reference signals (V1 and V2) and the previously detected test packets, for HH polarization. It can be seen that the $\max|\rho|$ for the filtered reference V2 practically doubles the value of the original reference signal, and that V1 is slightly worse than V2 (on the order of 10% on average).

Figure 6 shows these results for VV polarization. It can be seen that the performance is similar.

This improvement in performance is expected from what was observed in the PSDs of Fig. 4. It should be noted that here we take the correlation coefficient as the performance indicator, since it measures the similarity between the signals; a higher value of the modulus of ρ indicates a reference signal that describes more accurately the received signal. This improvement in the description of the reference signal will impact on a better performance of the detection of interfering signals.

To make a fair performance analysis, the interval considered for the correlation is the one that would correspond to the preamble of the test packages (according to their theoretical length) plus 35% of previous samples and 35% of subsequent samples. In other words, we search in the temporal dimension to find the maximum of $|\rho|$.

In the calculus of correlation we also incorporate the frequency error, Δ_f. That is, we also search in the frequency dimension to find the maximum of $|\rho|$. To do this search, we add different frequency error values on the previously described reference signals (that is, already filtered if applicable). An alternative (perhaps more realistic) approach would be to incorporate the error before filtering the signals, which is computationally more expensive, and with which we have not obtained significant improvements.

Figure 7 shows the frequency error for which the maximum is observed in each case for the HH polarization. It can be seen that there is consistency between the frequency error values in which the maximum occurs for the three reference signals considered. These frequency error values (as well as their dispersion) partly explain the groups observed in Fig. 3, although not conclusively. The results for the VV polarization are similar and there is consistency between the values obtained for both polarizations, but it is not shown due to space restrictions.

V. Conclusion

In this work we present a method of identifying the processing that weather radar performs on incoming signals. We show how, by means of this identification, two reference signals can be built that closely resembles the preambles of the test data packets. This close resemblance, expressed in terms of the

value of the modulus of the correlation coefficient, allows us, on the one hand, to affirm that the assumption of the linear phase LTI system model is appropriate. On the other hand, this enables to improve the detection of interfering Wi-Fi signals.

It is important to clarify that to implement the detection strategy, the correlation that this same system imposes on the output noise must be taken into account [23]. As can be seen from the estimated PSD, Fig. 2, this noise is no longer white. For this, it is possible to use the same receiver identification that is done in this work. The design of the detection algorithm is outside the scope of this article and will be considered in future work.

As an intermediate result, we also developed a simple ad-hoc interference detection technique based on power levels, which is therefore independent of the signal structure. With this technique we obtained the packets used as tests.

It should also be noted that although the improvement in the correlation coefficient when incorporating the effect of filtering is notable, the values obtained are still of the order of 20% below the observed correlation coefficient between the test packets themselves (in mean, considering the maximum correlation between each packet and any other one).

This means that the design of the reference signal could be further improved. From what is used in this work, three places are identified in which this improvement could be focused: in the first place, in analyzing or better modeling the behavior of the receiver phase, for which the preambles themselves could be used, once they have been detected; in second place, other alternatives should be analyzed to incorporate the decimation; and in third place, the stage where the correction of the frequency error is incorporated. So far we have not found interesting results in these lines, and they are considered as future work.

It should also be clarified that the need to identify the receiver is due to the fact that in our research projects we have access to the data but not to the detailed design of the receiver (except for a few details that have been stated). Of course, for this identification, as well as for the design of interference detection strategies, it would be of great interest to have the digital samples prior to the processing carried out by the matched filter, in which we also plan to advance in the future.

ACKNOWLEDGMENT

This work was supported in part by the Universidad Nacional de Río Negro under Grants PI-JI 40-B-899 and PIDTT 40-B-693, in part by the Universidad Nacional de Cuyo under Grant C038 4142/19, in part by the Agencia Nacional de promoción Científica y Tecnológica under Grant PICT-2018-01277, in part by the Consejo Nacional de Investigaciones Científicas y Técnicas (CONICET) and in part by the Comisión Nacional de Energía Atómica (CNEA).

RMA data was provided by Secretaría de Infraestructura y Políticas Hídricas, Ministerio del Interior, Obras Públicas y Vivienda of the Argentinean National Government framed within the SINARAME Project. The National System of Weather Radars (Sistema Nacional de Radares Meteorológicos, SINARAME) project is an Argentinean effort to expand the radar network over the whole country.

REFERENCES

[1] A. V. Ryzhkov and D. S. Zrnić, *Radar Polarimetry for Weather Observations*. Springer International Publishing, 2019.

[2] R. J. Doviak and D. S. Zrnić, *Doppler Radar and Weather Observations, 2nd Ed.* Academic Press, 1993.

[3] https://www.invap.com.ar/en/divisions/defense-security-and-environment/c-band-weather-radar/.

[4] E. Saltikoff, J. Y. N. Cho, P. Tristant, A. Huuskonen, L. Allmon, R. Cook, E. Becker, and P. Joe, "The threat to weather radars by wireless technology," *Bulletin of the American Meteorological Society*, vol. 97, no. 7, pp. 1159 – 1167, 2016.

[5] B. H. Walke, S. Mangold, and L. Berlemann, *IEEE 802 Wireless Systems: Protocols, Multi-Hop Mesh / Relaying, Performance and Spectrum Coexistence*. Wiley, 2007.

[6] P. Joe, J. Scott, J. Sydor, A. B. ao, and A. Yongacoglu, "Radio local area network (RLAN) and c-band weather radar interference studies," in *32nd AMS Radar Conference on Radar Meteorology, Albuquerque, New Mexico, Oct 24-29*, 2005.

[7] J. E. Carroll, F. H. Sanders, R. L. Sole, and G. A. Sanders, "Case study: Investigation of interference into 5 ghz weather radars from unlicensed national information infrastructure devices, part i," NTIA Technical Report TR-11-473, Tech. Rep., 2010.

[8] M. Vaccarono, C. V. Chandrasekar, R. Bechini, and R. Cremonini, "Survey on electromagnetic interference in weather radars in northwestern italy," *Environments*, vol. 6, no. 12, 2019.

[9] V. N. Bringi and V. Chandrasekar, *Polarimetric Doppler weather radar: principles and applications*, 1st ed. 40 West 20th Street, New York: Cambridge University Press, 2004.

[10] L. Rojas, D. N. Moisseev, V. Chandrasekar, J. Selzler, and R. Keränen, "Dual-polarization spectral filter for radio frequency interference suppression," in *Seventh European Conference on Radar in Meteorology and Hydrology (ERAD 2012)*, 2012.

[11] R. Keränen, L. Rojas, and P. Nyberg, "Progress in mitigation of WLAN interferences at weather radar," in *36th Conf. on Radar Meteorology, Breckenridge, CO, Amer. Meteor. Soc., 336.*, 2013.

[12] J. Y. N. Cho, "A new radio frequency interference filter for weather radars," in *Journal of Atmospheric and Oceanic Technology, Vol. 34*, Jul. 2017.

[13] Q. Cao and M. Knight, "Mitigation of radio frequency pulse interference on dual-pol weather radar," in *American Meteorological Society 99th annual meeting*, Jan. 2019, pp. 6–10.

[14] G. O. Petracca, "Estudio e implementación de métodos de eliminación de interferencias WLAN/RLAN en radares meteorológicos," Master's thesis, Universidad Nacional de Crdoba, 2017.

[15] R. J. González, "Eliminación de interferencias WLAN/RLAN en imágenes de radar meteorológico mediante la implementación de wavelets y otros filtros discretos," Trabajo Final Integrador, Universidad Nacional de Ro Negro, 2020.

[16] O. Barba Leal, "Caracterización y detección de interferencia WLAN/RLAN en radares meteorológicos," Proyecto Integrador de Grado, Instituto Balseiro, Universidad Nacional de Cuyo., 2019.

[17] O. Barba Leal, F. Rinalde, J. Cogo, and J. P. Pascual, "Detección de señales WLAN en registros de datos de radar meteorolóogico," 2021, article accepted to be published in RPIC 2021.

[18] A. Papoulis and S. U. Pillai, *Probability, Random Variables, and Stochastic Processes*. McGraw-Hill, 2002.

[19] B. Porat, *A Course in Digital Signal Processing*. Wiley, 1997.

[20] I. Ivić and T. S., "Online determination of noise level in weather radars," in *Preprints, 27th Conf. on Interactive Information and Processing Systems (IIPS), Seattle, WA, Amer. Meteor. Soc.*, 2011.

[21] L. B. G. and C. S., *Broadband Wireless Access and Local Networks. Mobile WiMAX and WiFi*. Artech House, 2008.

[22] "IEEE standard 802.11. wireless LAN medium access control (MAC) and physical layer (PHY) specifications." 2016.

[23] S. M. Kay, *Fundamentals of Statistical Signal Processing: Detection theory*. Prentice-Hall PTR, 1998.